The MEK5–ERK5 Kinase Axis Controls Lipid Metabolism in Small-Cell Lung Cancer

Sandra Cristea[1,2], Garry L. Coles[1,2], Daniel Hornburg[2], Maya Gershkovitz[1,2], Julia Arand[1,2], Siqi Cao[1,2], Triparna Sen[3], Stuart C. Williamson[1,2,4], Jun W. Kim[1,2], Alexandros P. Drainas[1,2], Andrew He[1,2], Laurent Le Cam[5], Lauren Averett Byers[3], Michael P. Snyder[2], Kévin Contrepois[2], and Julien Sage[1,2]

ABSTRACT

Small-cell lung cancer (SCLC) is an aggressive form of lung cancer with dismal survival rates. While kinases often play key roles driving tumorigenesis, there are strikingly few kinases known to promote the development of SCLC. Here, we investigated the contribution of the MAPK module MEK5–ERK5 to SCLC growth. MEK5 and ERK5 were required for optimal survival and expansion of SCLC cell lines *in vitro* and *in vivo*. Transcriptomics analyses identified a role for the MEK5–ERK5 axis in the metabolism of SCLC cells, including lipid metabolism. In-depth lipidomics analyses showed that loss of MEK5/ERK5 perturbs several lipid metabolism pathways, including the mevalonate pathway that controls cholesterol synthesis. Notably, depletion of MEK5/ERK5 sensitized SCLC cells to pharmacologic inhibition of the mevalonate pathway by statins. These data identify a new MEK5–ERK5–lipid metabolism axis that promotes the growth of SCLC.

Significance: This study is the first to investigate MEK5 and ERK5 in SCLC, linking the activity of these two kinases to the control of cell survival and lipid metabolism.

Introduction

Small-cell lung cancer (SCLC) is a subtype of lung cancer characterized by features of neuroendocrine differentiation, rapid growth, and a high metastatic potential. More than 200,000 patients die from SCLC every year worldwide. As smoking rates increase in several parts of the world, the number of patients developing and succumbing to SCLC continues to grow. Patients with SCLC are usually treated with a combination of radiotherapy and chemotherapy. However, resistant tumors usually emerge within months; at this point, therapeutic options are very limited, leading to the dismal survival rates of this disease (reviewed in refs. 1, 2). Recent observations indicate that immunotherapies may help treat subsets of patients with SCLC (3). Similarly, targeting DNA repair pathways may prove useful to induce cell death in SCLC cells and inhibit the growth of SCLC tumors (4). Nonetheless, it is critical to identify and investigate additional therapeutic options, requiring a deeper understanding of SCLC biology, and the pathways underlying its tumorigenicity.

Resection of SCLC is rare, which, for many years, has limited the number of samples available for analysis. More recently, however, a global effort among multiple groups resulted in a more substantial collection of SCLC samples, and an investigation of the genetic and genomic events that may drive the growth of SCLC (5–7). A notable genetic feature of SCLC is that the recurrent mutations observed are often loss-of-function events that inactivate tumor suppressors, including nearly ubiquitous inactivation of the *RB1* and *TP53* tumor suppressor genes. A few oncogenic drivers have been identified, including transcription factors such as MYC family members and NFIB. Some of these gain- and loss-of-function events have been validated as drivers of SCLC growth in genetically engineered mouse models and human cells and may represent new therapeutic opportunities, including c-Myc (8) or CREBBP (9). However, the striking rarity of reoccurring oncogenic driving mutations points to the existence of unexplored key vulnerabilities in SCLC (5–7).

The dysregulation of kinase signaling is an essential driver of oncogenic growth in multiple contexts (10). SCLC tumors have very few activating events in genes coding for kinases (reviewed in ref. 11). Nevertheless, work on kinases implicated in the response to DNA damage, including WEE1 and CHK1 (12–14), shows that such kinases are promising targets in this disease. There is little evidence for a role for canonical MAPK signaling (MEK1–ERK1/2) in SCLC (11), but the less-studied MEK5–ERK5 kinase axis has not yet been investigated in SCLC oncogenesis. In other cancers, the MEK5–ERK5 axis has been observed to play roles in many different pathways, with multiple phenotypic results, and these two kinases have emerged as possible therapeutic targets (reviewed in refs. 15–17). This dual kinase axis is responsible for increased growth or metastasis, lower overall survival, or resistance to therapies in multiple tumor types, including breast cancer (16, 18–20), prostate cancer (21), colon cancer (18), hepatocellular carcinomas (18, 21), and high-grade osteosarcomas (18). Overall, however, the molecular mechanisms and intracellular consequences of MEK5 and ERK5 actions leading to these cancer phenotypes are not well understood. Here we sought to investigate the role of these two kinases in SCLC. We found that MEK5 and ERK5 play a critical role for the survival of SCLC cells. We also determined that

[1]Department of Pediatrics, Stanford University, Stanford, California. [2]Department of Genetics, Stanford University, Stanford, California. [3]Department of Thoracic/Head and Neck Medical Oncology, The University of Texas MD Anderson Cancer Center, Houston, Texas. [4]Clinical and Experimental Pharmacology Group, Cancer Research UK Manchester Institute, Manchester, United Kingdom. [5]IRCM, Institut de Recherche en Cancérologie de Montpellier, INSERM, Université de Montpellier, Institut Régional du Cancer de Montpellier, Montpellier, France.

Note: Supplementary data for this article are available at Cancer Research Online (http://cancerres.aacrjournals.org/).

Current address for T. Sen: Memorial Sloan Kettering Cancer Center, New York, New York.

Corresponding Author: Julien Sage, Stanford University School of Medicine, 269 Campus Drive, SIM1 G2078, Stanford, CA 94305. Phone: 650-723-0195; Fax: 650-736-0195; E-mail: julsage@stanford.edu

Cancer Res 2020;80:1293–303

doi: 10.1158/0008-5472.CAN-19-1027

MEK5 and ERK5 control lipid metabolism in SCLC cells, including cholesterol metabolism, suggesting possible future therapeutic avenues for SCLC treatment.

Materials and Methods

Ethics statement

Mice were maintained according to practices prescribed by the NIH at Stanford's Research Animal Facility accredited by the American Association for Accreditation of Laboratory Animal Care. All animal studies were conducted following approval from the Stanford Animal Care and Use Committee.

In vivo growth assays

Cells to be injected were stained for viability with Trypan Blue solution (Sigma-Aldrich catalog no. T8154) and counted using a Countess II FL Automated Cell Counter. One million cells were injected subcutaneously per flank of each NSG mouse, in 100 μL RPMI media without any serum or antibiotics, and 100 μL Corning Matrigel Matrix (Phenol red-free). Tumors were then monitored for growth, and mice were sacrificed at 21 days postinjection. Tumors were measured by caliper, and tumor volume was calculated using the formula $(4\pi/3)((\text{length}+\text{width})/4))^3$. Each cell line was injected into both flanks for 2 different mice. When graphing, the volumes of tumors on different flanks of the same mouse were averaged.

Cell culture

SCLC cell lines were maintained and passaged as described before (22). All cell lines were passaged and grown in RPMI1640 media supplemented with 10% bovine growth serum (BGS; Thermo Fisher Scientific; unless stated as 2% serum), and penicillin-streptomycin–glutamine (Gibco). These cells grow as suspension spheres or aggregates in culture. All cell lines were maintained at 37°C in a humidified chamber with 5% CO_2. KP1 murine SCLC cells and NJH29 human SCLC cells have previously been described (5). All cell lines were routinely tested for *Mycoplasma* (MycoAlert Mycoplasma Detection Kit, Lonza, LT07-418) and all the cells used in this study were negative. Mouse cell lines were derived from mouse tumors and genotyped for genetic loss of Rb and p53. Human cell lines were purchased from ATCC (except for NJH29, which was developed at Stanford University from a SCLC patient) and not further authenticated.

Proliferation assays, cell cycle and cell death assays, gene knockdown, and gene expression were performed largely as before (22). See Supplementary Methods file for details.

Atorvastatin treatment and IC_{50} assays

Atorvastatin Calcium (Selleckchem, #S2077) was dissolved in DMSO as per manufacturer's instructions. A total of 2×10^4 cells of each cell line treated were plated per well of a 96-well plate, in 90 μL of reduced (2% BGS) serum media, in triplicate for each treatment condition. Cells were allowed to reform their spheroids (in the case of mSCLC KP1 cells) or clumps (in the case of many hSCLC cells) or to adhere (in the case of some hSCLC cell lines, such as SBC5) for 24 hours, after which, a 10× concentration of atorvastatin or vehicle control (DMOS) in 2% BGS media was added to each well, in a 10 μL volume for a total volume of 100 μL per well. Forty-eight hours or 5 days later, plates were read using the AlamarBlue reagent (Thermo Fisher Scientific, DAL1100), as described above. Atorvastatin was used at final concentrations of 0 (DMSO only), 2, 5, 10 and 20 μmol/L. The fraction of remaining viable cells was calculated by dividing the averaged fluorescence signal of each concentration replicate set for each cell line, by the vehicle control averaged values for that same cell line.

For atorvastatin IC_{50} assays on MEK5/ERK5-knockdown cells, hSCLC NJH29 cells were plated similarly, at 2×10^4 cells per well of a 96-well plate, for each shRNA-expressing sample, in 90 μL of reduced (2% BGS) serum media, in triplicate for each treatment condition. Plates were read using AlamarBlue after 48 hours of atorvastatin treatment, and. IC_{50} values were calculated using GraphPad Prism 7.

Immunoassays

Protein levels were determined by immunoblot or using the Simple Western quantitative immunoassay and the Compass software, according to the manufacturer's protocol. Cells were lysed in RIPA lysis buffer from Thermo Fisher Scientific (catalog no. 89900), supplemented with proteasome and phosphatase inhibitors, and lysates were cleared by centrifugation at maximum speed for 10 minutes, and sonicated for 30 seconds each. Total protein was quantified using the Pierce BCA Protein Assay Kit (Thermo Fisher Scientific, catalog no. 23277). For Simple Western, whole-cell lysates were diluted to a final concentration of 0.2 μL/mL. For Simple Western immunoassays, the antibodies and dilutions used were as follows: ERK5 (D23E9) rabbit mAb (Cell Signaling Technology, #3552, 1:100), ERK5 (D3I5V) rabbit mAb (Cell Signaling Technology, #12950, 1:50) phospho-ERK5 (Thr218/Tyr220) rabbit polyclonal antibody (Cell Signaling Technology, #3371, 1:50), PCNA (PC10) mouse mAb (Cell Signaling Technology, #2586, 1:100), cleaved PARP (D124) rabbit mAb (Cell Signaling Technology, #9664, 1:100), Tubulin mouse mAb, (Sigma-Aldrich T9026, 1:500), HSP90 (C45G5) rabbit mAb (Cell Signaling Technology, #4877, 1:10,000), NEUROD1 (D35G2) rabbit mAb (Cell Signaling Technology, #4373, 1:2000), and MASH1/ASCL1 mouse mAb (BD Biosciences, #556604, 1:1,000). All other conditions and reagents were as suggested by the manufacturer. A representative example of quantification with raw data is shown in Supplementary Table S16. For immunoblot, washing was done in Tris-buffered saline washing buffer with 0.1% Tween-20, blocking was done with 10% milk in washing buffer, and antibodies were diluted in 5% milk in washing buffer. Antibodies used in immunoassays were as follows: MEK5 mouse mAb antibody (sc-135986, 1:1,000), HMGCR rabbit mAb (Abcam, ab174830, 1:500), CC3 (D175) rabbit polyclonal antibody (Cell Signaling Technology, #9541, 1:100) HSP90 rabbit mAb (Cell Signaling Technology, #4877, 1:10,000), and peroxidase-AffiniPure goat anti-Rabbit IgG antibody (Jackson Immuno-Research, #111-035-144, 1:10,000).

Reverse-phase protein array

Human SCLC NJH29 cells were infected with lentiviral constructs expressing an shRNA against MEK5 and two independent shRNAs against ERK5 as well as two control shRNAs (shGFP and shSCR). These samples were infected, selected, expanded, and grown in reduced serum media (2% BGS) for 3–4 days in independent triplicates, Lysates were prepared as required by the MD Anderson Reverse-Phase Protein Array (RPPA) facility as reported previously (23), and submitted to the facility, where RPPA processing and statistical analysis was performed as before (23). Fold change values are shown unlogged, and *P* values are from simple Student *t* test calculations, with all replicates of shRNAs against MEK5 in one group, against ERK5 in another group, and against "controls" (shGFP and shSCR) in an "shCTRL" group.

RNA-seq library preparation, RNA-seq analysis, and gene set enrichment analysis

mSCLC KP1 cells and hSCLC NJH29 cells were grown in RPMI1640 media supplemented with 10% bovine growth serum (BGS; Thermo Fisher Scientific) and penicillin–streptomycin–glutamine (Gibco). After infection with respective lentiviral shRNA constructs in triplicate, the cells were subjected to 4 days of puromycin selection (Thermo Fisher catalog no. A1113803, 2 μg/mL for mSCLC cells and 2.5 μg/mL for hSCLC cells), then allowed to recover for 1–2 days without puromycin, and expanded for 3-4 days in 2% serum RPMI media. The details of RNA extraction, library preparation, sequencing, and analysis can be found in the Supplementary Methods file.

Lipid staining and lipidomics

Lipid staining was performed with BODIPY 493/503 dye (4,4-Difluoro-1,3,5,7,8-Pentamethyl-4-Bora-3a,4a-Diaza-s-Indacene, Thermo Fisher Scientific, #D3922) according to the manufacturer's instructions. Details can be found in the Supplementary Methods file.

Sample preparation

mSCLC KP1 cells were infected with two hairpins per gene (MEK5 and ERK5), as well as two control hairpins (shGFP and shSCR), in completely independent triplicates. These samples were subjected to selection and recovery, and allowed to expand in 2% BGS media. Cells were trypsinized and counted, and 10^7 live cells per sample were washed three times with 10 mL PBS, and snap-frozen in Eppendorf Safe-Lock 2 mL tubes (Eppendorf, # 022363344) by dropping in liquid nitrogen. Cell pellets were then stored at −80°C until further processing. The details of lipid extraction, measurements, and analysis can be found in the Supplementary Methods file.

DepMap analysis

Dependency scores for all assayed genes in all 25 hSCLC cell lines were extracted from the complete Combined RNAi (Broad, Novartis, Marcotte) dataset available on the Cancer Dependency Map website, downloaded from the Data tab (depmap.org/portal/download/) in August of 2018. Pearson correlations between the dependency scores of MEK5 and ERK5, respectively, and those of all other genes across the hSCLC cell lines, were calculated using the corrplot R package. These sets of genes were then compared with find genes with dependency scores that correlated "highly" ($r > 0.5$) with both MEK5 and ERK5 dependencies in hSCLC cell lines. The resulting 63 genes were then analyzed with Enrichr (amp.pharm.mssm.edu/Enrichr/) to find GO Molecular Functions, GO Biological Processes, KEGG Pathways, and WikiPathways lists, as well as statistical significance for each term.

REVIGO analysis

MEK5 and ERK5 dependency correlated genes were analyzed by Enrichr as stated above; GO Biological Processes terms associated with the 63 genes overlapping for MEK5 and ERK5 (Supplementary Table S10) were then analyzed and visualized using REVIGO (revigo.irb.hr/). GO ID numbers and P_{adj} values were entered into the REVIGO field, and analysis was performed with "Medium (0.7)" allowed similarity, the Homo sapiens GO database, and the SimRel (default) semantic similarity measure. The resulting scatterplot is shown with slight aesthetic changes, and only GO terms with dispensability scores < 0.05 are labeled.

Statistical analysis

Statistical significance was assayed with the GraphPad Prism 7 software. *, $P < 0.05$; **, $P < 0.01$; ***, $P < 0.001$; ****, $P < 0.0001$; ns, not significant. The tests used are indicated in the figure legends. To compare growth curves, we used the two-way ANOVA followed by *t* tests. When comparing more than two groups, we first performed one-way ANOVA, followed by *t* tests. If F-test for variance showed a significantly different distribution between two groups being compared (F-test $P < 0.05$), the nonparametric Mann–Whitney *P* value is reported instead of the Student *t* test *P* value, with significance symbols as described above. Data are represented as mean±SD unless otherwise stated. To calculate the significance of the overlap between two groups of genes, the hypergeometric test was used (systems.crump.ucla.edu/hypergeometric/index.php), with the "population size" being the sum of all genes identified after filtering, regardless of *P* value "number of successes in population" being the size of one list being considered (list 1), "sample size" being the size of the second list being overlapped (list 2), and "number of successes" being the overlap between list 1 and list 2.

Results

Depletion of MEK5 or ERK5 inhibits the expansion of SCLC cell populations

Surveying the data from the RNAi Cancer Dependency Map (24), we found that the majority of the 25 human SCLC cell lines tested show some dependency on *MAP2K5*, the gene coding for MEK5 (Supplementary Fig. S1A). The Cancer Dependency Map analysis in SCLC cell lines for *MAPK7*, coding for ERK5, showed little to no dependency (see depmap.org), suggesting that MEK5 may have additional targets in SCLC cells or that ERK5 loss is easier to compensate for in SCLC cells. Both *MAP2K5* and *MAPK7* are expressed at intermediate levels in human SCLC tumors (Supplementary Table S1). Data from the cBioPortal show occasional genetic events implicating the *MAP2K5* and *MAPK7* genes, with no reported recurrent events in SCLC but a missense mutation in the *MAPK7* gene (A501D) in 2 of 88 patients with adrenocortical carcinoma, suggestive of a possible oncogenic role for this kinase in neuroendocrine cancers (see cbioportal.org).

These observations and the absence of published data on MEK5–ERK5 in SCLC prompted us to further investigate the role of MEK5 and ERK5 in this form of lung cancer. To this end, we first knocked down these two kinases in mouse and human SCLC cells with independent sets of shRNA molecules (Supplementary Fig. S1B and S1C). Upon knockdown of the MEK5–ERK5 axis, human SCLC (hSCLC) NJH29 cells, and murine SCLC (mSCLC) KP1 cell populations grew slower compared with cells expressing control shRNAs (**Fig. 1A** and **B**; Supplementary Fig. S1D). As expected, phosphorylated ERK5 was downregulated when MEK5 was knocked down (Supplementary Fig. S1E). We also performed subcutaneous tumor growth assays in immunocompromised NOD-Scid-Gamma (NSG) mice and found that injection of MEK5- or ERK5-depleted cells resulted in lower tumor volumes compared with control knockdown cells (**Fig. 1C** and **D**). There was no evidence of counter-selection for the MEK5 knockdown in the context of these experiments (Supplementary Fig. S1F). Thus, the MEK5 and ERK5 kinases contribute to the optimal expansion of SCLC cell populations in culture and *in vivo*.

Depletion of MEK5 or ERK5 induces cell death in SCLC cell populations

The long-term growth of SCLC cells is driven by lineage transcription factors such as ASCL1 or NEUROD1 implicated in neuroendocrine identity (reviewed in ref. 25). We investigated whether MEK5 and ERK5 regulate the levels of these proteins. However, protein levels of ASCL1 were not affected by the loss of MEK5 in the ASCL1-high

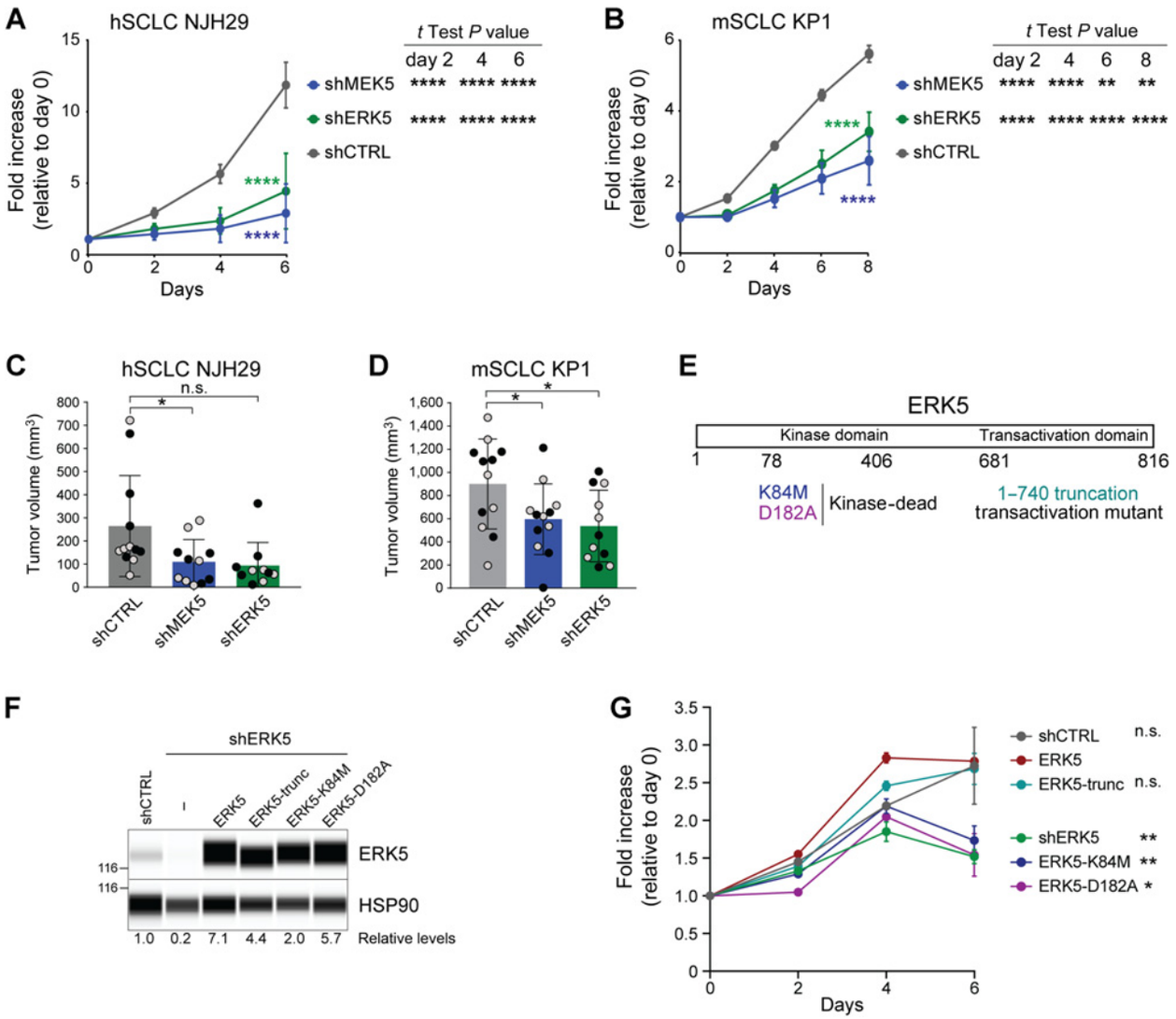

Figure 1.

MEK5 and ERK5 knockdown inhibits the expansion of SCLC cells. **A** and **B,** Quantification of populations growth in reduced serum (2%) of human NJH29 SCLC cells (**A**) and murine KP1 SCLC cells (**B**) with shRNA-mediated knockdown of MEK5 and ERK5 compared with shCTRLs by AlamarBlue assay. Two-way ANOVA $P_{interaction}$ values comparing the knockdown curves with the control are shown in colors; *t* test *P* values shown at the right of each graph specify comparison of each knockdown control, with **, $P < 0.01$; ***, $P < 0.001$; ****, $P < 0.0001$; $n = 2$ independent shRNAs per group (for hSCLC NJH29, $n = 5$–6 and for mSCLC KP1, $n = 3$ independent experiments per individual hairpin). **C** and **D,** Volume of tumors resulting from subcutaneous injections of hSCLC NJH29 cells (**C**) or mSCLC KP1 cells (**D**) expressing shMEK5, shERK5, or shCTRL (shGFP and shSCR) after 3 weeks of growth in the flanks of NSG recipient mice; gray and black dots represent two independent shRNAs per group ($n = 4$–6 independent experiments per individual hairpin). *, $P < 0.05$; n.s., nonsignificant, $P > 0.05$ by *t* test following one-way ANOVA ($P = 0.0192$ for **C** and $P = 0.0318$ for **D**). **E,** Schematic representation of the ERK5 protein with the mutants used in **F** and **G**. **F,** Immunoassays for ERK5 and HSP90 (loading control) in hSCLC NJH29 cells with ERK5 knockdown and re-expression of wild-type or mutant forms of ERK5, as indicated. Levels of ERK5 relative to HSP90 are indicated below. The 116 kDa molecular weight marker is shown on the left. **G,** Quantification of populations growth in reduced serum (2%) of human NJH29 SCLC cells as in **B** by AlamarBlue assay ($n = 3$). Two-way ANOVA *P* values comparing the kinase-dead mutants to the wild-type ERK5 rescue are significant ($P < 0.0001$ for both K84M and D182A); *t* test *P* values shown on the right are day 6 values compared with ERK5 rescue, with *, $P < 0.05$; **, $P < 0.01$; n.s., nonsignificant.

KP1 cells, and levels of NEUROD1 increased upon MEK5 loss in NEUROD1-high NJH29 cells (Supplementary Fig. S2A and S2B). These results suggested that the inhibition of SCLC growth upon reduction of the MEK5–ERK5 axis was not directly connected to these transcription factors and neuroendocrine cell identity.

ERK5 is a kinase that can also function as a transcription activator (26, 27). To determine the function(s) of ERK5 that are important for the expansion of SCLC cells, we reintroduced into ERK5 knockdown NJH29 human SCLC cells either wild-type ERK5 or mutant forms of ERK5 with impaired transcriptional or kinase activities (**Fig. 1E** and **F**). The inhibition of growth observed upon ERK5 knockdown was rescued by wild-type ERK5 as well as by a truncation mutant that abolishes the transcriptional activity; in contrast, two separate kinase-dead mutant failed to rescue the growth defects (**Fig. 1G**), indicating that ERK5 kinase activity is important for the optimal growth of SCLC cell populations in this context.

On the basis of these observations, to further investigate the role of the MEK5–ERK5 axis in SCLC, we next queried a number of signaling pathways, many mediated by phosphocascades, using an RPPA approach (28) in MEK5 and ERK5 knockdown cells. Following this antibody-based functional proteomic analysis, unsupervised clustering grouped MEK5 and ERK5 knockdown cells together, while control cells had distinct profiles, indicating that MEK5 and ERK5 belong to the same phosphocascade in SCLC cells (**Fig. 2A**; Supplementary Fig. S2C and S2D; Supplementary Table S2). However, few major concerted changes were identified in specific signaling pathways in MEK5 and ERK5 knockdown cells compared with controls. One exception was changes in proteins implicated in apoptotic cell death, such as increased detection of cleaved caspase-7, cleaved PARP, and the proapoptotic factor BIM, upon MEK5/ERK5 depletion. Consistent with these findings, MEK5 and ERK5 knockdown cells showed a higher propensity toward apoptotic cell death in culture (**Fig. 2B** and **C**). No significant changes were observed in cell-cycle profiles under the same conditions in culture (Supplementary Fig. S2E and S2F). When we examined markers of cell-cycle progression and cell death *in vivo* in xenografts from NJH29 cells upon ERK5 knockdown, we found no obvious changes in PCNA, a marker of DNA replication, and a trend toward increased cleaved PARP and cleaved caspase-3, two markers of apoptotic cell death (**Fig. 2D**–**F**; Supplementary Fig. S2G). Together, these observations indicate that the MEK5–ERK5 axis controls the expansion of SCLC cells mainly by promoting their survival.

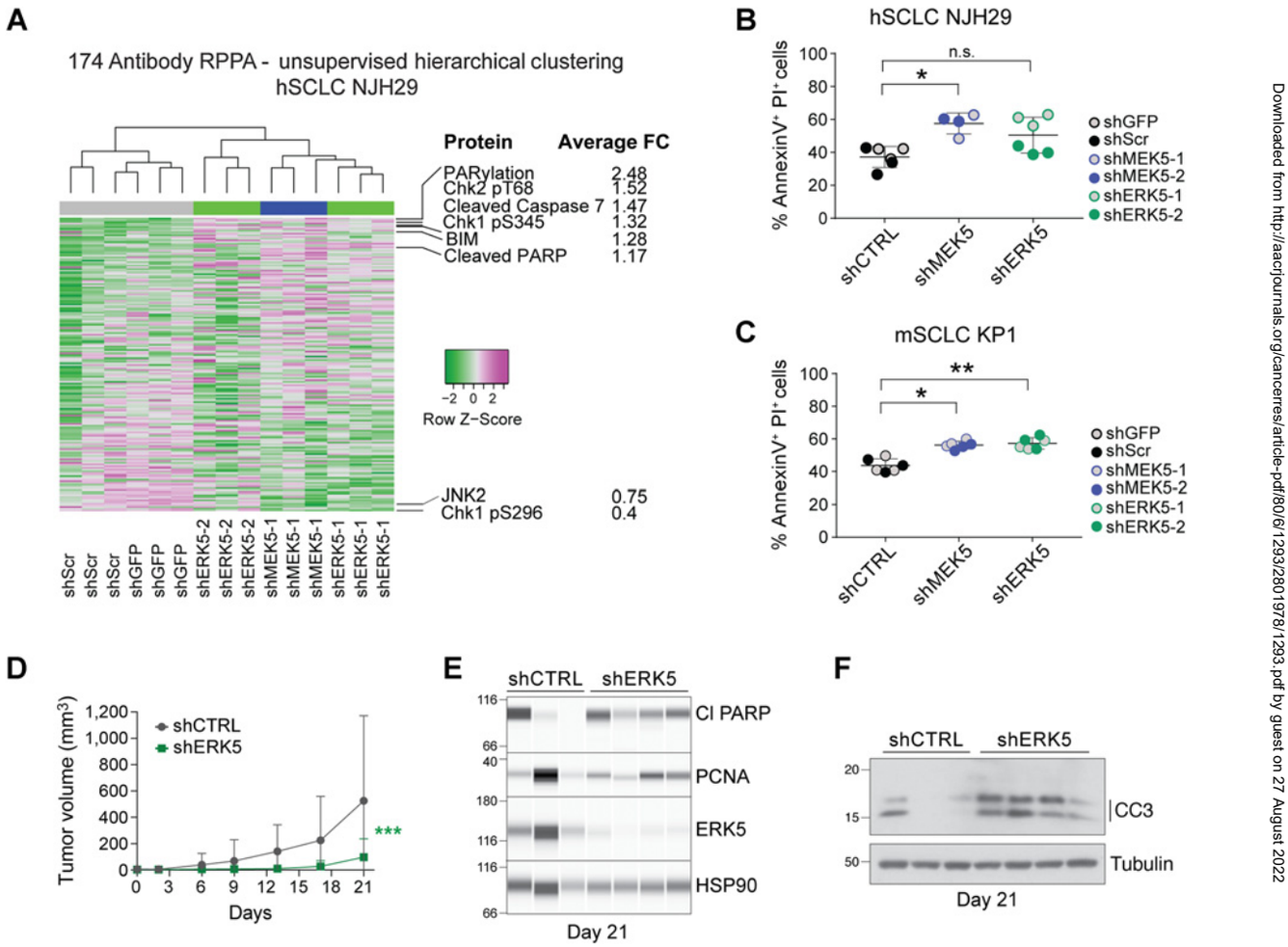

Figure 2.

MEK5 and ERK5 knockdown induces cell death in SCLC cell populations. **A,** Unsupervised hierarchical clustering of all protein quantities measured by RPPA separates hSCLC NJH29 cells with MEK5 and ERK5 knockdown from those with shCTRL knockdowns (shGFP and shSCR; top); for proteins with average fold change (FC) across all ERK5 and MEK5 hairpins larger than 1.15 or smaller than 0.75, protein names and average fold changes are noted. **B** and **C,** Knockdown of MEK5 and ERK5 in hSCLC NJH29 (**B**) and mSCLC KP1 (**C**) SCLC cells results in a higher rate of cell death by apoptosis as measured by AnnexinV/PI staining and flow cytometry after 2 days of growth in 2% serum conditions. n.s., nonsignificant, $P > 0.05$; *, $P < 0.05$; **, $P < 0.01$ by t test following one-way ANOVA ($P = 0.0115$ for **B** and $P = 0.004$ for **D**); gray and colored dots represent two different shRNAs per group, and $n = 2$–3 independent experiments per individual hairpin. **D,** Volume of tumors resulting from subcutaneous injections of hSCLC NJH29 cells expressing shERK5 (one shRNA) or shCTRL (shGFP) during 3 weeks of growth in the flanks of NSG recipient mice ($n = 12$ tumors per group; error bars, SEM). Two-way ANOVA, ***, $P_{interaction} = 0.0002$. **E,** Immunoassays for ERK5, the cell death marker cleaved PARP (Cl PARP), and the cell-cycle marker PCNA on extracts from NJH29 tumors in **D** at day 21 of growth. Tumors were selected to minimize differences due to tumor size ($n = 3$ shCTRL and $n = 4$ shERK5). HSP90 was used as a loading control. **F,** Immunoblot as in **E** for the cell death marker cleaved caspase-3 (CC3). Tubulin was used as a loading control.

Depletion of MEK5 or ERK5 perturbs gene programs associated with metabolic pathways

To gain further insights into the mechanisms by which the MEK5 and ERK5 proteins promote the survival and the expansion of SCLC cell populations, we performed transcriptional RNA-seq analyses of SCLC cells with an impaired MEK5–ERK5 axis (Supplementary Fig. S3A; Supplementary Tables S3 and S4). In unsupervised hierarchical clustering analyses (**Fig. 3A**) and principal component analysis (PCA) of the gene expression data (Supplementary Fig. S3B), mSCLC KP1 cells with MEK5 and ERK5 knockdown clustered separately from controls; similarly, MEK5 knockdown hSCLC NJH29 cells clustered separately from control cells (**Fig. 3A**; Supplementary Fig. S3A and S3B). ERK5 knockdown NJH29 cells were not investigated using this assay. A significant overlap was found between the genes downregulated upon MEK5 knockdown in KP1 and NJH29 cells, suggesting that MEK5 has a similar role in promoting gene expression programs in these two contexts (Supplementary Fig. S3C). In addition, the programs affected by MEK5 and ERK5 knockdown overlapped significantly in KP1 cells, confirming that the two kinases, indeed, function in the same phosphocascade (**Fig. 3B**). Gene set enrichment analysis (GSEA) of averaged $\log_2$-fold change values in murine MEK5 and ERK5 knockdown SCLC cells indicated

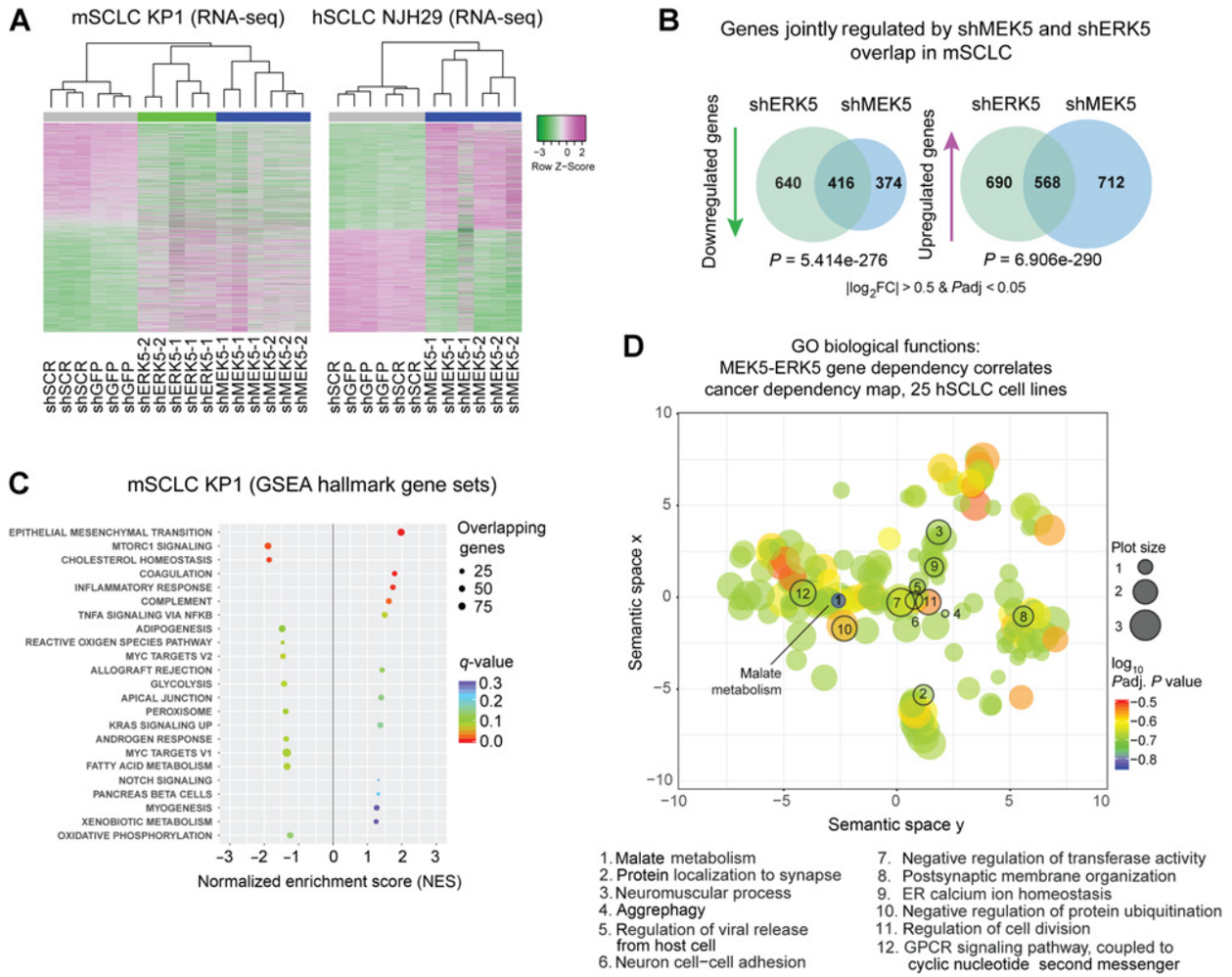

Figure 3.

MEK5 and ERK5 knockdown perturbs metabolic pathways in SCLC cells. **A,** Unsupervised clustering from RNA-seq data upon MEK5/ERK5 knockdown in mSCLC KP1 cells and MEK5 knockdown in hSCLC NJH29 cells; all genes with $|\log_2$ fold change$|>0.5$ and P_{adj} values < 0.05 were included in the analysis from any comparison; $n =$ 2–3 independent replicates per hairpin. **B,** MEK5 and ERK5 knockdown in mSCLC KP1 cells change the transcriptome in similar ways, with significantly overlapping gene sets being downregulated and upregulated; hypergeometric test used to obtain P value of overlap; only genes changing by a $|\log_2$ fold change$| > 0.5$ and an P_{adj} < 0.05 were considered. **C,** Hallmarks GSEA gene sets significantly enriched or disenriched when the MEK5–ERK5 axis was downregulated in mSCLC KP1 cells compared with controls; $\log_2$-fold change values averaged for shMEK5 and shERK5, respectively, each compared with shCTRLs (shGFP and shSCR) to focus analysis on genes controlled by both kinases; only enriched sets with q values < 0.3 are shown. **D,** Gene Ontology Biological Function term results from Enrichr, for the set of 63 genes with a Pearson correlation coefficient of over 0.5 between their dependency scores and those of both MEK5 and ERK5 in 25 hSCLC cell lines from the Cancer Dependency Map project, analyzed by ReviGO, and mapped on the basis of their semantic similarity; GO IDs with a dispensability score < 0.15 are numbered and stated in the legend below; bubble or plot size is proportional to frequency of Homo sapiens UniProt entries associated with that GO ID; color specifies $\log_{10} P_{adj}$ value for that GO ID from Enrichr.

downregulation of metabolic pathways upon reduction of MEK5 and ERK5 levels (**Fig. 3C**; Supplementary Table S5). Similar metabolic pathways were found downregulated at the transcriptional level in NJH29 cells upon MEK5 knockdown (Supplementary Fig. S3D; Supplementary Table S6). Neither mSCLC nor hSCLC cells with MEK5–ERK5 axis knockdown showed an enrichment in cell-cycle or neuroendocrine genes (Supplementary Fig. S4A and S4B), further supporting that the loss of viability of SCLC cells after MEK5/ERK5 depletion is not due to a change in neuroendocrine status or their proliferation rate.

We also investigated the genes whose dependency scores were most correlated with those for MEK5 or ERK5 in the 25 human SCLC cell lines of the Cancer Dependency Map project. 298 and 293 genes had a dependency score Pearson correlation coefficient greater than 0.5 for MEK5 and ERK5, respectively, with an overlap of 63 genes (Supplementary Table S7). Enrichr analysis of these 63 genes confirmed a link between MEK5 and ERK5 and metabolic pathways, with the most significant GO Molecular Functions terms suggesting links to malate metabolism and phosphofructokinase activity (Supplementary Table S8); GO Biological Process analysis further highlighted malate metabolism, NADH metabolism, oxaloacetate metabolism, and Vitamin D biosynthesis (Supplementary Table S9 and summarized by REVIGO analysis in **Fig. 3D** and Supplementary Table S10). KEGG pathway analysis and WikiPathways highlighted connections between MEK5–ERK5 signaling and pyruvate metabolism and glyoxylate and dicarboxylate metabolism, as well as the citrate cycle and glycolysis (Supplementary Tables S11 and S12).

Together, this analysis of transcriptional networks and dependency links loss of MEK5 or ERK5 in SCLC cells to perturbations in metabolism. In particular, a number of genes and pathways found to be altered in the RNA-seq and Cancer Dependency Map analyses of MEK5–ERK5 deficient SCLC cells pointed to lipid metabolism–related pathways, including those implicated in cholesterol homeostasis and *de novo* fatty acid (FA) synthesis. These data suggest that altered metabolism, including lipid metabolism, may contribute to decreased survival and growth inhibition upon inactivation of the MEK5–ERK5 module.

MEK5 and ERK5 knockdown affects cholesterol synthesis pathways

Little to nothing is known about lipid metabolism in SCLC and the connection between the MEK5–ERK5 axis and lipid homeostasis (29, 30). Consistent with our findings, one of the most significant transcription factor target gene sets to be identified by GSEA as disenriched in MEK5 and ERK5-deficient cells, was SREBP (Sterol-Regulatory Element Binding Protein) target genes (Supplementary Fig. S5A; Supplementary Table S13). Indeed, SREBP targets (31) were downregulated in MEK5-deficient human and murine cells and ERK5-deficient murine cells (**Fig. 4A**; Supplementary Fig. S5B). Briefly, the SREBP pathway has two arms, including the mevalonate pathway regulated by SREBF2, which results in cholesterol synthesis, and the

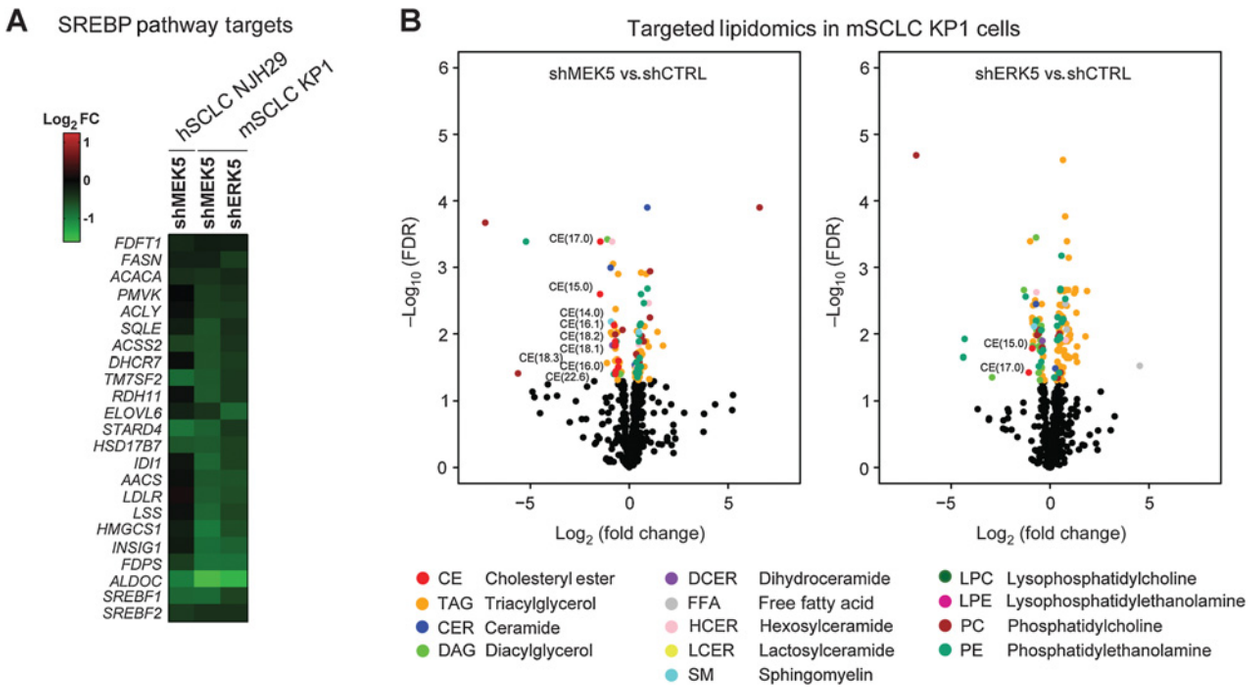

Figure 4.

MEK5 and ERK5 loss changes the lipidomic profile of SCLC cells. **A,** MEK5 and ERK5 knockdown cells downregulate SREBP pathway targets compared with cells infected with shCTRLs (from RNA-seq FPM values). **B,** Significantly changing lipid species ($P < 0.05$) between shMEK5 and shCTRL cells (left) or between shERK5 and shCTRL cells (right) are shown in volcano plots with -$\log_{10}$(FDR) on the *y*-axis and $\log_2$-fold change on the *x*-axis; significantly changing lipid species (FDR < 0.05) are shown as colored dots according to their lipid classes (colors corresponding to different lipid classes are shown in the legend at bottom); significantly changing cholesteryl esters (CE) are labeled with their number of carbons and unsaturations contained on the fatty acid moeity. TAG, triacylglycerols; CER, ceramides; DAG, diacylglycerols; DCER, dihydrocermides; FFA, free fatty acids; HCER, hexosylceramides; LCER, lactosylceramindes; SM, sphingomyelins; LPC, lysophosphatidylcholines; LPE, lysophosphatidylethanolamines; PC, phosphatidylcholines; PE, phosphatidylethanolamines. n = 2–3 independent replicates per hairpin.

fatty acid synthesis pathway regulated by SREBF1 (32). Staining of MEK5 and ERK5 knockdown cells with BODIPY showed no significant decrease in total neutral lipid content compared with controls (Supplementary Fig. S5C). To more specifically ascertain which components of lipid synthesis were dysregulated following MEK5 and ERK5 knockdown, we subjected murine SCLC cells (KP1) to targeted lipidomics analyses (**Fig. 4B**; Supplementary Fig. S5D; Supplementary Tables S14 and S15). Unsupervised hierarchical clustering and PCA clustered MEK5 and ERK5 knockdown SCLC cells separately from controls (Supplementary Fig. S6A). In addition, though multiple lipid species were changing significantly, the only lipid classes to show all significantly changing species as reduced in abundance in both MEK5 and ERK5 knockdown cells were cholesteryl esters (CE), diacylglycerols (DAG) and dihydroceramides (DCER; **Fig. 4B**; Supplementary Fig. S6B). Out of the classes with relative decreased abundance as a consequence of MEK5/ERK5 knockdown, the DCER lipid class was represented by a single specific DCER significantly downregulated in both MEK5 and ERK5 knockdown samples (Supplementary Fig. S6B). Among the remaining two classes, decreased CE abundance was predominant in MEK5 knockdown cells, while DAG was the lipid class predominantly downregulated in ERK5 knockdown cells. Free fatty acids (FFA) were not significantly altered in MEK5–ERK5 knockdown cells; in addition, although the relative abundance of a diverse range of triacylglycerol (TAG) species, into which FAs are incorporated for energy storage, changed, they did so in both directions (**Fig. 4B**; Supplementary Tables S14 and S15). In contrast, the relative abundance of all detected CEs was significantly decreased in MEK5-knockdown mSCLC KP1 cells, and several were also reduced in ERK5-knockdown cells (Supplementary Fig. S6C, see also Methods and Supplementary Fig. S6D). Together, these data point to cholesterol biosynthesis pathways downstream of MEK5–ERK5 and suggest that these metabolic defects could contribute to the loss of viability of SCLC cells upon MEK5 or ERK5 depletion.

Inhibition of the MEK5–ERK5 axis and the mevalonate pathway can both limit the expansion of SCLC cells

The mevalonate pathway is composed of a sequence of enzymatic steps that convert Acetyl-CoEnzymeA into cholesterol and isoprenoids (33). Consistent with our lipidomic analyses, genes encoding enzymes involved in different steps of this pathway were downregulated by shMEK5 in human and murine SCLC cells, and by shERK5 in murine SCLC cells (**Fig. 5A**; Supplementary Fig. S7A). One of the most clinically relevant inhibitors of this pathway is atorvastatin calcium (known commercially as Lipitor; ref. 34), an inhibitor of the rate-limiting enzyme HMG-CoA-Reductase (HMGCR). HMGCR levels were lower in MEK5 and ERK5 knockdown cells at the RNA level (**Fig. 5A**). HMGCR protein levels were also lower in ERK5 knockdown cells (**Fig. 5B**). To evaluate the importance of the mevalonate pathway in SCLC, we first treated 8 cell lines [7 hSCLC and 1 mSCLC cell line (KP1)] with low micromolar doses of atorvastatin for 2 or 5 days. Atorvastatin decreased viability by an average of 50% across the human SCLC cell lines and approximately 60% in mouse KP1 cells after 2 days of treatment, with a decreased viability of approximately 80% by day 5 (**Fig. 5C**). These results are in line with the inhibitory activity of two related compounds, simvastatin and fluvastatin on hSCLC cell lines in a recent large-scale screening effort (Supplementary Fig. S7B; ref. 35).

These data identifying a previously unknown connection between the MEK5–ERK5 axis and the mevalonate pathway in SCLC cells led us to test the possibility that inhibiting both pathways simultaneously may have a greater effect on the expansion of SCLC cells than the inhibition of each single pathway. We focused on the NJH29 cell line, one of the most resistant to atorvastatin treatment in our study. Strikingly, ERK5 depletion in NJH29 cells sensitized these cells to further inhibition of the mevalonate pathway by low doses of atorvastatin (**Fig. 5D**; Supplementary Fig. S7C). These experiments further strengthened the functional link between the MEK5–ERK5 axis and the mevalonate pathway in SCLC.

Discussion

SCLC is a disease with a dire survival rate reflective of late diagnosis, incredibly quick metastasis, few and ineffective treatment choices, and an underlying lack of knowledge about its basic biology. Here we focused on the relatively unexplored MEK5–ERK5 axis, a pathway that is not recurrently altered at the genetic level but that we hypothesized could be a driving force in SCLC. Accumulating evidence supports an important role for MEK5 and ERK5 in various phenotypes associated with cancer, even though the protumorigenic effects of these two enzymes have not been associated with genetic events leading to their activation (15–17). We identified a prosurvival role for these kinases in SCLC cells and show that they are implicated in the control of cholesterol synthesis and other lipid metabolism pathways in SCLC cells.

We identified a prosurvival role for these kinases in SCLC cells. A similar role in the control of survival has been described for MEK5 and ERK5 in multiple normal and cancerous cell types (21, 36, 37), suggesting that this function is broadly conserved for the MEK5–ERK5 axis. The upstream signals that activate MEK5 and ERK5 remain poorly understood, especially in the context of prosurvival signals in cancer cells. The downstream mechanisms by which this kinase axis promotes survival are also poorly understood but likely to be diverse. Our work and recent work by others suggest that it may include the regulation of metabolic pathways. A recent study identified a link between MEK5/ERK5 and the stability of MYC, a regulator of cell metabolism and growth (38); this link is corroborated by our RNA-seq analysis (**Fig. 3C**). Emerging evidence also links MEK5 and ERK5 to the control of oxidative phosphorylation (39). Notably, one study makes a connection between forced oxidative phosphorylation and downstream effects on cholesterol levels, via an increase in LDLR expression and intracellular LDL-cholesterol intake–a process dependent on the MEK5–ERK5 axis (29). To our knowledge, however, there is no prior direct description of a control of *de novo* cholesterol synthesis by the MEK5–ERK5 axis. Further studies are required to determine whether our observation is specific to SCLC or if it applies to other cell types. Importantly, our data show that the lipid metabolism phenotypes of MEK5 loss and ERK5 loss are very similar, but not identical, in SCLC cells, and it is thus also possible that some of the mechanisms of survival control are different for the two kinases. Notably, our results suggest that the kinase activity of ERK5 contributes to its protumorigenic role in SCLC, and inhibitors of both kinases in the pathway may provide therapeutic strategies in the future, especially in combination with other therapeutic agents.

Our work also highlights the current general lack of knowledge of SCLC metabolism. SCLC, like many tumors, is thought to be highly glycolytic. However, unlike most cancers, which predominantly express the PKM2 isoform of pyruvate kinase M, a glycolytic enzyme that specifies the fate of glucose-derived carbons, SCLC cells express a higher ratio of PKM1 to PKM2 (40). This results in SCLC cells having higher glucose flux into lactate conversion and the TCA cycle, attenuated glutamine metabolism, and likely being better at performing mitophagy, and attaining lower ROS (reactive oxygen species)

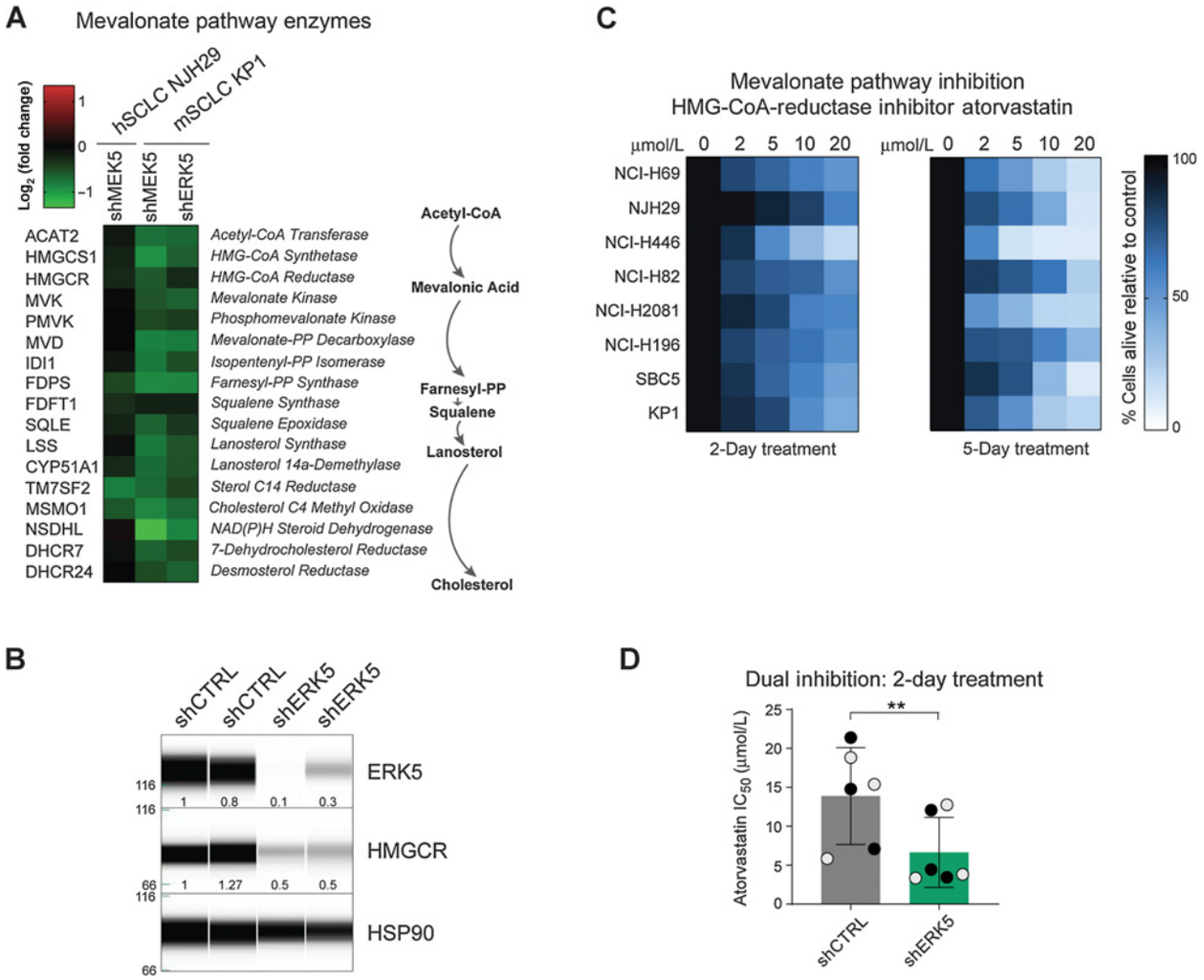

Figure 5.

MEK5 and ERK5 knockdown results in inhibition of the mevalonate pathway and increased sensitivity to mevalonate pathway inhibitors. **A,** MEK5 and ERK5 knockdown cells downregulate mevalonate pathway enzymes (biosynthesis schematic on right) compared with cells infected with shCTRL hairpins (from RNA-seq FPM values). **B,** Immunoassay for ERK5, HMGCR, and HSP90 expression in control and ERK5 knockdown NJH29 hSCLC cells. The molecular weights are indicated on the left (in kDa). The amount of ERK5 and HMGCR relative to the first control and to HSP90 is indicated below the signal corresponding to each protein. **C,** Treatment of 8 SCLC cell lines (7 human cell lines and the mouse cell line KP1) with increasing doses of atorvastatin in reduced (2%) serum media; color corresponds to percent cells alive compared with vehicle-treated controls after 2 or 5 days at each concentration; $n = 3$ independent experiments per treatment. **D,** Concentrations of atorvastatin necessary to kill 50% of NJH29 cells (IC_{50}) infected with shCTRLs are higher than concentrations needed to kill cells with ERK5 knockdown; gray and black dots represent two independent hairpins per group; $n = 3$ experiments. **, $P \leq 0.005$, t test.

levels (41). Another recent study shows that the ASCL1-low subtype of SCLC tumors is specifically dependent on *de novo* purine synthesis *in vivo* (42).

While large amounts of lipids have been demonstrated to be necessary to support the rapid proliferation of cancer cells, the implication of lipid metabolism in SCLC remains poorly understood. A single study utilizing metabolomic profiling of one SCLC cell line (NCI-H446) found elevated carnitine palmitoyltransferase 1A (CPT1A) and 2 (CPT2), key enzymes in fatty acid oxidation, compared with NSCLC and normal epithelial cell controls (43). The only SCLC study to date related to cholesterol metabolism, to our knowledge, is a correlative study that found that low serum LDL (low-density lipoprotein), and low protein expression of LDLR (low-density lipoprotein receptor), both independently correlate with better overall survival (44). A previous study using simvastatin, a pharmacologic inhibitor of HMCGR, the rate-limiting enzyme of the mevalonate pathway, in SCLC cell lines observed a decrease in proliferation, but linked these effects to possible changes in RAS signaling and not to general cholesterol metabolism (45). Our studies provide novel insights into lipid biology in SCLC cells and comparisons with future analyses in other cancer types will identify unique aspects of lipid metabolism in SCLC cells. For example, SCLC cells have been observed to require lipid-raft mediated SRC-PI3K/AKT activation for sustained growth in culture (46). In addition, the isoprenoid byproducts of the mevalonate pathway are crucial for the prenylation of multiple proteins (including RAS superfamily members), which is critical for their correct tethering, localization, and protein–protein binding signaling functions (47). Furthermore, cholesterol itself can be attached directly to proteins,

including Smoothened (SMO) in the Hedgehog pathway, a pathway that has been shown to control SCLC tumor initiation and progression (48, 49). These cholesterol-mediated functions regulate a wide range of cellular processes, including cell polarity and cell body dynamics, cell proliferation and survival, protein and intracellular vesicular trafficking, cell cycle, and nuclear transport dynamics–all of which may affect the survival and the expansion of SCLC cells.

Targeting the mevalonate pathway as a therapeutic intervention is being investigated in multiple tumor types (50). Our experiments exposing SCLC cell lines to atorvastatin suggest that at least a subset of SCLC cells is sensitive to HMGCR inhibition. Interestingly, a few clinical trials have included patients with SCLC treated with statins (45, 51, 52), with no visible benefit for the survival of these patients. However, given the evidence building up that HMGCR inhibitors such as statins have multiple effects, systemically and tumor specifically, the failure of these trials may say more about the complexity of cholesterol inhibition in tumors and in human tissues than it does about the degree of dependence of SCLC on cholesterol synthesis. Consistent with our findings, a recent study identified sensitivity to inhibition of the cholesterol biosynthetic pathway enzyme squalene epoxidase in SCLC cells (53). A large meta-analysis of small cell neuroendocrine tumors also suggests susceptibility to disruption of lipid and sterol metabolism (54). Additional investigation into the latter will need to be performed to ascertain which of the many roles of the mevalonate pathway and its byproducts are truly critical in SCLC.

Our work suggests that the anticancer effects of inhibiting the mevalonate pathway may be enhanced by inhibition of the MEK5–ERK5 axis, which may be achieved when potent and specific inhibitors of these kinases have been developed (55). In addition, mevalonate pathway inhibitors were found to have vaccine-adjuvant activities and to synergize with anti-PD-1 antibodies to kill tumor cells, by enhancing the functions of antigen-presenting cells (56). Therefore, mevalonate pathway inhibition may also have the ability to increase antigen presentation to the immune system, perhaps serving as a future adjuvant for an SCLC vaccine in conjunction with FDA-approved immunotherapies.

In this study, we present the first experiments suggesting that a less-studied arm of the MAPK pathway, the MEK5–ERK5 dual kinase axis, is crucial for sustained SCLC cell viability. Furthermore, we have connected this axis to downstream cholesterol biology in SCLC, especially the mevalonate pathway. Additional experiments need to be performed to identify the detailed molecular mechanism of these connections, but our studies already present multiple single and combinatorial therapeutic strategies, which can be further tested and validated preclinically, in hopes of clinical success for the hundreds of thousands of patients who die yearly from SCLC.

Disclosure of Potential Conflicts of Interest

L.A. Byers reports receiving a commercial research grant from AstraZeneca and Sierra Oncology and is a consultant/advisory board member for AstraZeneca, Sierra Oncology, PharmMar, SA, and AbbVie. M.P. Snyder is a cofounder and a member of SAB at Personalis, has received speakers bureau honoraria from Guardant and has ownership interest (including patents) in Personais, Q Bio, January, Filtricine, SensOmics, and Protos. J. Sage reports receiving a commercial research grant from StemCentrx/Abbvie, Revolution Medicines and has ownership interest (including patents) in Forty Seven Inc. No potential conflicts of interest were disclosed by the other authors.

Authors' Contributions

Conception and design: S. Cristea, L.L. Cam, J. Sage
Development of methodology: S. Cristea, T. Sen, A.P. Drainas, L.A. Byers
Acquisition of data (provided animals, acquired and managed patients, provided facilities, etc.): S. Cristea, G.L. Coles, D. Hornburg, T. Sen, S.C. Williamson, A. He, L.A. Byers, K. Contrepois
Analysis and interpretation of data (e.g., statistical analysis, biostatistics, computational analysis): S. Cristea, D. Hornburg, J. Arand, S. Cao, T. Sen, A. He, L.A. Byers, K. Contrepois, J. Sage
Writing, review, and/or revision of the manuscript: S. Cristea, D. Hornburg, S. Cao, T. Sen, S.C. Williamson, J.W. Kim, L.L. Cam, L.A. Byers, K. Contrepois, J. Sage
Administrative, technical, or material support (i.e., reporting or organizing data, constructing databases): S. Cristea, G.L. Coles, D. Hornburg, M. Gershkovitz, M.P. Snyder, J. Sage
Study supervision: M.P. Snyder, J. Sage
Other (lipidomics experimental design, biochemistry, mass spectrometry, and data analysis): D. Hornburg

Acknowledgments

This work was supported by the Department of Defense (grant W81XWH-15-1-0250 to J. Sage), the NIH (grants R01CA206540, R01CA201513, U01CA213273, and R35CA231997 to J. Sage; grant F31CA206346 to S. Cristea; grant CA16672 to MD Anderson RPPA facility; grant 3P50HG00773505S1 to M.P. Snyder), the American Cancer Society (ACS) postdoctoral fellowship (to G.L. Coles), the National Science Foundation Graduate Research Fellowship (to S. Cao), a CRUK-Fulbright scholarship (to S.C. Williamson), the Emerson Collective (to J. Sage), the Lung Cancer Research Foundation (LCRF; to T. Sen), a CRUK-Fulbright scholarship (to S.C. Williamson), and the UICC (Union for International Cancer Control) Yamagiwa Yoshida Memorial International study fund and Cancéropôle Grand Sud Ouest (to L.L. Cam). J. Sage is the Harriet and Mary Zelencik Scientist in Children's Cancer and Blood Diseases. We thank the staff of the Stanford Functional Genomics Facility, the FACS Core at the Institute for Stem Cell Biology and Regenerative Medicine, and the Stanford Veterinary Service Center, as well as Pauline Chu, for their technical support and expertise. We acknowledge members of the Sweet-Cordero and Sage laboratories for technical and materials support, including Andrea Chaikovsky for her help with immunoblots.

The costs of publication of this article were defrayed in part by the payment of page charges. This article must therefore be hereby marked *advertisement* in accordance with 18 U.S.C. Section 1734 solely to indicate this fact.

Received April 16, 2019; revised December 13, 2019; accepted January 13, 2020; published first January 22, 2020.

References

1. Bunn PA Jr., Minna JD, Augustyn A, Gazdar AF, Ouadah Y, Krasnow MA, et al. Small cell lung cancer: can recent advances in biology and molecular biology be translated into improved outcomes? J Thorac Oncol 2016;11:453–74.
2. Sabari JK, Lok BH, Laird JH, Poirier JT, Rudin CM. Unravelling the biology of SCLC: implications for therapy. Nat Rev Clin Oncol 2017;14:549–61.
3. Horn L, Mansfield AS, Szczesna A, Havel L, Krzakowski M, Hochmair MJ, et al. First-line atezolizumab plus chemotherapy in extensive-stage small-cell lung cancer. N Engl J Med 2018;379:2220–9.
4. Pietanza MC, Waqar SN, Krug LM, Dowlati A, Hann CL, Chiappori A, et al. Randomized, double-blind, phase II study of temozolomide in combination with either veliparib or placebo in patients with relapsed-sensitive or refractory small-cell lung cancer. J Clin Oncol 2018;36:2386–94.
5. George J, Lim JS, Jang SJ, Cun Y, Ozretic L, Kong G, et al. Comprehensive genomic profiles of small cell lung cancer. Nature 2015;524:47–53.
6. Peifer M, Fernandez-Cuesta L, Sos ML, George J, Seidel D, Kasper LH, et al. Integrative genome analyses identify key somatic driver mutations of small-cell lung cancer. Nat Genet 2012;44:1104–10.
7. Rudin CM, Durinck S, Stawiski EW, Poirier JT, Modrusan Z, Shames DS, et al. Comprehensive genomic analysis identifies SOX2 as a frequently amplified gene in small-cell lung cancer. Nat Genet 2012;44:1111–6.

8. Mollaoglu G, Guthrie MR, Bohm S, Bragelmann J, Can I, Ballieu PM, et al. MYC drives progression of small cell lung cancer to a variant neuroendocrine subtype with vulnerability to aurora kinase inhibition. Cancer Cell 2017;31:270–85.
9. Jia D, Augert A, Kim DW, Eastwood E, Wu N, Ibrahim AH, et al. Crebbp loss drives small cell lung cancer and increases sensitivity to HDAC inhibition. Cancer Discov 2018;8:1422–37.
10. Knapp S, Sundstrom M. Recently targeted kinases and their inhibitors-the path to clinical trials. Curr Opin Pharmacol 2014;17C:58–63.
11. Cristea S, Sage J. Is the canonical RAF/MEK/ERK signaling pathway a therapeutic target in SCLC? J Thorac Oncol 2016;11:1233–41.
12. Sen T, Tong P, Stewart CA, Cristea S, Valliani A, Shames DS, et al. CHK1 inhibition in small cell lung cancer produces single-agent activity in biomarker-defined disease subsets and combination activity with cisplatin or olaparib. Cancer Res 2017;77:3870–84.
13. Sen T, Tong P, Diao L, Li L, Fan Y, Hoff J, et al. Targeting AXL and mTOR pathway overcomes primary and acquired resistance to WEE1 inhibition in small-cell lung cancer. Clin Cancer Res 2017;23:6239–53.
14. Lallo A, Frese KK, Morrow C, Szczepaniak Sloane R, Gulati S, Schenk MW, et al. The combination of the PARP inhibitor olaparib and the Wee1 inhibitor AZD1775 as a new therapeutic option for small cell lung cancer. Clin Cancer Res 2018;24:5153–64.
15. Wang X, Tournier C. Regulation of cellular functions by the ERK5 signalling pathway. Cell Signal 2006;18:753–60.
16. Hoang VT, Yan TJ, Cavanaugh JE, Flaherty PT, Beckman BS, Burow ME. Oncogenic signaling of MEK5-ERK5. Cancer Lett 2017;392:51–9.
17. Stecca B, Rovida E. Impact of ERK5 on the hallmarks of cancer. Int J Mol Sci 2019; 20. DOI: 10.3390/ijms20061426.
18. Simoes AE, Rodrigues CM, Borralho PM. The MEK5/ERK5 signalling pathway in cancer: a promising novel therapeutic target. Drug Discov Today 2016;21: 1654–63.
19. Liu F, Zhang H, Song H. Upregulation of MEK5 by Stat3 promotes breast cancer cell invasion and metastasis. Oncol Rep 2017;37:83–90.
20. Antoon JW, Martin EC, Lai R, Salvo VA, Tang Y, Nitzchke AM, et al. MEK5/ERK5 signaling suppresses estrogen receptor expression and promotes hormone-independent tumorigenesis. PLoS One 2013;8:e69291.
21. Lochhead PA, Gilley R, Cook SJ. ERK5 and its role in tumour development. Biochem Soc Trans 2012;40:251–6.
22. Denny SK, Yang D, Chuang CH, Brady JJ, Lim JS, Gruner BM, et al. Nfib promotes metastasis through a widespread increase in chromatin accessibility. Cell 2016;166:328–42.
23. Byers LA, Wang J, Nilsson MB, Fujimoto J, Saintigny P, Yordy J, et al. Proteomic profiling identifies dysregulated pathways in small cell lung cancer and novel therapeutic targets including PARP1. Cancer Discov 2012;2:798–811.
24. Tsherniak A, Vazquez F, Montgomery PG, Weir BA, Kryukov G, Cowley GS, et al. Defining a cancer dependency map. Cell 2017;170:564–76 e16.
25. Rudin CM, Poirier JT, Byers LA, Dive C, Dowlati A, George J, et al. Molecular subtypes of small cell lung cancer: a synthesis of human and mouse model data. Nat Rev Cancer 2019;19:289–97.
26. Kasler HG, Victoria J, Duramad O, Winoto A. ERK5 is a novel type of mitogen-activated protein kinase containing a transcriptional activation domain. Mol Cell Biol 2000;20:8382–9.
27. Nithianandarajah-Jones GN, Wilm B, Goldring CE, Muller J, Cross MJ. ERK5: structure, regulation and function. Cell Signal 2012;24:2187–96.
28. Tibes R, Qiu Y, Lu Y, Hennessy B, Andreeff M, Mills GB, et al. Reverse phase protein array: validation of a novel proteomic technology and utility for analysis of primary leukemia specimens and hematopoietic stem cells. Mol Cancer Ther 2006;5:2512–21.
29. Khan AUH, Allende-Vega N, Gitenay D, Gerbal-Chaloin S, Gondeau C, Vo DN, et al. The PDK1 inhibitor dichloroacetate controls cholesterol homeostasis through the ERK5/MEF2 pathway. Sci Rep 2017;7:10654.
30. Belkahla S, Haq Khan AU, Gitenay D, Alexia C, Gondeau C, Vo DN, et al. Changes in metabolism affect expression of ABC transporters through ERK5 and depending on p53 status. Oncotarget 2018;9:1114–29.
31. Horton JD, Shah NA, Warrington JA, Anderson NN, Park SW, Brown MS, et al. Combined analysis of oligonucleotide microarray data from transgenic and knockout mice identifies direct SREBP target genes. Proc Natl Acad Sci U S A 2003;100:12027–32.
32. Guo D, Bell EH, Mischel P, Chakravarti A. Targeting SREBP-1-driven lipid metabolism to treat cancer. Curr Pharm Des 2014;20:2619–26.
33. Buhaescu I, Izzedine H. Mevalonate pathway: a review of clinical and therapeutical implications. Clin Biochem 2007;40:575–84.
34. Jones P, Kafonek S, Laurora I, Hunninghake D. Comparative dose efficacy study of atorvastatin versus simvastatin, pravastatin, lovastatin, and fluvastatin in patients with hypercholesterolemia (the CURVES study). Am J Cardiol 1998;81: 582–7.
35. Polley E, Kunkel M, Evans D, Silvers T, Delosh R, Laudeman J, et al. Small cell lung cancer screen of oncology drugs, investigational agents, and gene and microRNA expression. J Natl Cancer Inst 2016;108. DOI: 10.1093/jnci/djw122.
36. Hayashi M, Kim SW, Imanaka-Yoshida K, Yoshida T, Abel ED, Eliceiri B, et al. Targeted deletion of BMK1/ERK5 in adult mice perturbs vascular integrity and leads to endothelial failure. J Clin Invest 2004;113:1138–48.
37. Watson FL, Heerssen HM, Bhattacharyya A, Klesse L, Lin MZ, Segal RA. Neurotrophins use the Erk5 pathway to mediate a retrograde survival response. Nat Neurosci 2001;4:981–8.
38. Vaseva AV, Blake DR, Gilbert TSK, Ng S, Hostetter G, Azam SH, et al. KRAS suppression-induced degradation of MYC Is antagonized by a MEK5-ERK5 compensatory mechanism. Cancer Cell 2018;34:807–22 e7.
39. Charni S, de Bettignies G, Rathore MG, Aguilo JI, van den Elsen PJ, Haouzi D, et al. Oxidative phosphorylation induces de novo expression of the MHC class I in tumor cells through the ERK5 pathway. J Immunol 2010;185:3498–503.
40. Morita M, Sato T, Nomura M, Sakamoto Y, Inoue Y, Tanaka R, et al. PKM1 confers metabolic advantages and promotes cell-autonomous tumor cell growth. Cancer Cell 2018;33:355–67 e7.
41. Nomura M, Morita M, Tanuma N. A metabolic vulnerability of small-cell lung cancer. Oncotarget 2018;9:32278–9.
42. Huang F, Ni M, Chalishazar MD, Huffman KE, Kim J, Cai L, et al. Inosine monophosphate dehydrogenase dependence in a subset of small cell lung cancers. Cell Metab 2018;28:369–82 e5.
43. Yu L, Li K, Xu Z, Cui G, Zhang X. Integrated omics and gene expression analysis identifies the loss of metabolite-metabolite correlations in small cell lung cancer. Onco Targets Ther 2018;11:3919–29.
44. Zhou T, Zhan J, Fang W, Zhao Y, Yang Y, Hou X, et al. Serum low-density lipoprotein and low-density lipoprotein expression level at diagnosis are favorable prognostic factors in patients with small-cell lung cancer (SCLC). BMC Cancer 2017;17:269.
45. Khanzada UK, Pardo OE, Meier C, Downward J, Seckl MJ, Arcaro A. Potent inhibition of small-cell lung cancer cell growth by simvastatin reveals selective functions of Ras isoforms in growth factor signalling. Oncogene 2006;25:877–87.
46. Arcaro A, Aubert M, Espinosa del Hierro ME, Khanzada UK, Angelidou S, Tetley TD, et al. Critical role for lipid raft-associated Src kinases in activation of PI3K-Akt signalling. Cell Signal 2007;19:1081–92.
47. Ahmadi Y, Ghorbanihaghjo A, Argani H. The balance between induction and inhibition of mevalonate pathway regulates cancer suppression by statins: A review of molecular mechanisms. Chem Biol Interact 2017;273:273–85.
48. Park KS, Martelotto LG, Peifer M, Sos ML, Karnezis AN, Mahjoub MR, et al. A crucial requirement for hedgehog signaling in small cell lung cancer. Nat Med 2011;17:1504–8.
49. Chen C, Breslin MB, Lan MS. Sonic hedgehog signaling pathway promotes INSM1 transcription factor in neuroendocrine lung cancer. Cell Signal 2018;46: 83–91.
50. Clendening JW, Penn LZ. Targeting tumor cell metabolism with statins. Oncogene 2012;31:4967–78.
51. Seckl MJ, Ottensmeier CH, Cullen M, Schmid P, Ngai Y, Muthukumar D, et al. Multicenter, phase III, randomized, double-blind, placebo-controlled trial of pravastatin added to first-line standard chemotherapy in small-cell lung cancer (LUNGSTAR). J Clin Oncol 2017;35:1506–14.
52. Ung MH, MacKenzie TA, Onega TL, Amos CI, Cheng C. Statins associate with improved mortality among patients with certain histological subtypes of lung cancer. Lung Cancer 2018;126:89–96.
53. Mahoney CE, Pirman D, Chubukov V, Sleger T, Hayes S, Fan ZP, et al. A chemical biology screen identifies a vulnerability of neuroendocrine cancer cells to SQLE inhibition. Nat Commun 2019;10:96.
54. Balanis NG, Sheu KM, Esedebe FN, Patel SJ, Smith BA, Park JW, et al. Pan-cancer convergence to a small-cell neuroendocrine phenotype that shares susceptibilities with hematological malignancies. Cancer Cell 2019;36:17–34 e7.
55. Nguyen D, Lemos C, Wortmann L, Eis K, Holton SJ, Boemer U, et al. Discovery and characterization of the potent and highly selective (Piperidin-4-yl) pyrido[3,2- d]pyrimidine based in vitro probe BAY-885 for the kinase ERK5. J Med Chem 2019;62:928–40.
56. Xia Y, Xie Y, Yu Z, Xiao H, Jiang G, Zhou X, et al. The mevalonate pathway is a druggable target for vaccine adjuvant discovery. Cell 2018;175:1059–73 e21.